LAWRENCE
LIVERMORE
NATIONAL
LABORATORY

UCRL-TR-218457

Concealed Threat Detection at Multiple Frames-per-second

J. T. Chang

January 27, 2006

Disclaimer

Auspices Statement

This work was performed under the auspices of the U. S. Department of Energy (DOE) by the University of California, Lawrence Livermore National Laboratory (LLNL) under Contract No. W-7405-Eng-48. The project (02-ERD-061) was funded by the Laboratory Directed Research and Development Program at LLNL.

FY04 LDRD Final Report
Concealed Threat Detection at Multiple Frames-per-second
LDRD Project Tracking Code: 02-ERD-061
John Chang, Principal Investigator

EXECUTIVE SUMMARY

Project Overiview

In this LDRD project, our research purpose is to investigate the science and technology necessary to enable real-time array imaging as a rapid way to detect hidden threats through obscurants such as smoke, fog, walls, doors, and clothing. The goal of this research is to augment the capabilities of protective forces in concealed threat detection. In the current context, threats include people as well as weapons. In most cases, security personnel must make very fast assessments of a threat based upon limited amount of data.

Among other attributes, UWB has been shown and quantified to penetrate and propagate through many materials (wood, some concretes, non-metallic building materials, some soils, etc.) while maintaining high range resolution. We have build collaborations with university partners and government agencies. We have considered the impact of psychometrics on target recognition and identification. Specifically we have formulated images in real-time that will engage the user's vision system in a more active way to enhance image interpretation capabilities.

Project goals

In this project, we are researching the use of real time (field programmable gate arrays) integrated with high resolution (cm scale), ultra wide band (UWB) electromagnetic signals for imaging personnel through smoke and walls. We evaluated the ability of real-time UWB imaging for detecting smaller objects, such as concealed weapons that are carried by the obscured personnel. We also examined the cognitive interpretation process of real time UWB electromagnetic images.

Accomplishments and Results

This project has been sponsored by the SEP Directorate and Engineering Directorate-Center of Non-Destructive Evaluation and ended in FY04. To meet the goals as described above, we have developed a numerical imaging algorithm and implemented it to study UWB beam forming and steering. We have been successful in developing a computational simulator system to evaluate and predict the performance of the imaging system. The simulator is capable of generating impulse radar images of moving targets with arbitrary trajectories. It is capable of facilitating parametric studies of the effects of transceiver element configuration. It has been used to guide us in anticipating and benchmarking

what information the laboratory prototype system should be acquiring and presenting.

Further, we have been successful in building the laboratory prototype radar camera hardware, and we subsequently used it to study and characterize the phenomena of UWB image generation. To that end, we have demonstrated a laboratory based imaging system that can represent images at approximately 15 frames per second. Real-time image analysis algorithms have undergone preliminary investigation, and software development based on those algorithms is continuing through other sponsored projects. In addition, we have collaborated with the DOD in characterizing the behavior of UWB electromagnetic signals through various building materials in order to assess the capability of imaging through such materials.

Examples of the laboratory prototype generated images are shown in Figure 1, demonstrating sample frames from UWB radar imaging of man holding a rifle 1 meter down range. Data collected using an effective 10x10 element array (realized through combined mechanical/electrical scanning using a linear 10 element array-8 transmitters and 2 receivers, with array aperture of 1.5mx1.5m). Current technology at a large spatial resolution (Figure 1 left) has demonstrated potential of 12 frames per second using the prototype system. The right image corresponded to a more complex and computationally intense reconstruction algorithm. Current technology has the potential of enabling 1 frame per 2 seconds to produce the higher resolution image on the right.

To evaluate the physical characteristics and limitations of using UWB signals for imaging, this project further quantified and demonstrated the effects of UWB beam forming and focusing ability. Figure 2 shows a case comparison of the effect of bandwidth on the ability to focus UWB signals. It clearly demonstrates that a large bandwidth is not only desired, but also required to enable focusing. This capability is a prerequisite to enable beam steering for image formation.

To evaluate the effect of array configuration that will enable beam steering, this project engaged into a parametric research on array geometry and radiating element distribution. As an example, Figure 3 demonstrates that an array configuration of interleaving transceivers suppresses sidelobe levels that in turn can enable a much better capability of image formation.

A provisional patent application has been put in place. The investigators have been active in attending national conferences, including invited talks. Also, we have briefed several internal programs and external customers on our concept and have received uniformly positive encouragement with several possible funding leads.

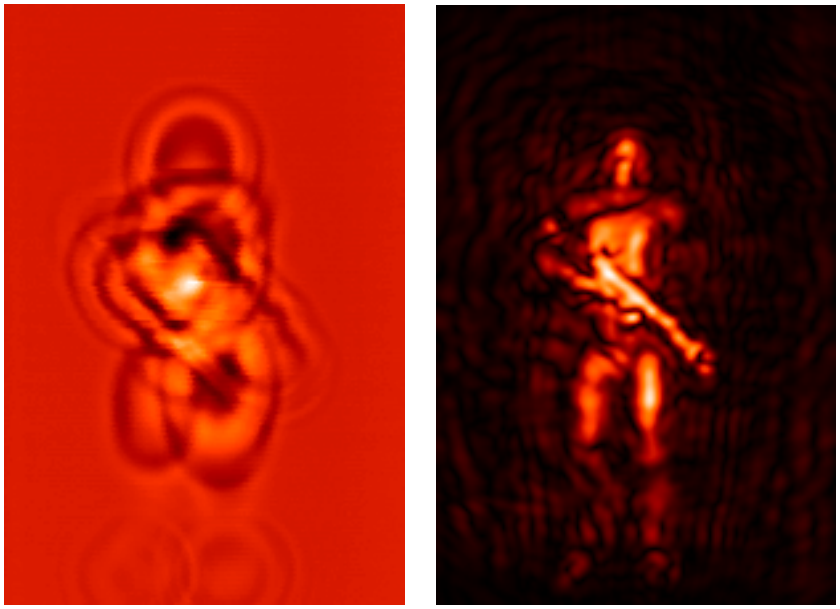

Figure1 Show sample frames from UWB radar imaging of a man holding a rifle 1 meter down range. The left image corresponding to a simple Hugh transform processed image. The right corresponded to a more complex and computationally intensive reconstruction algorithm.

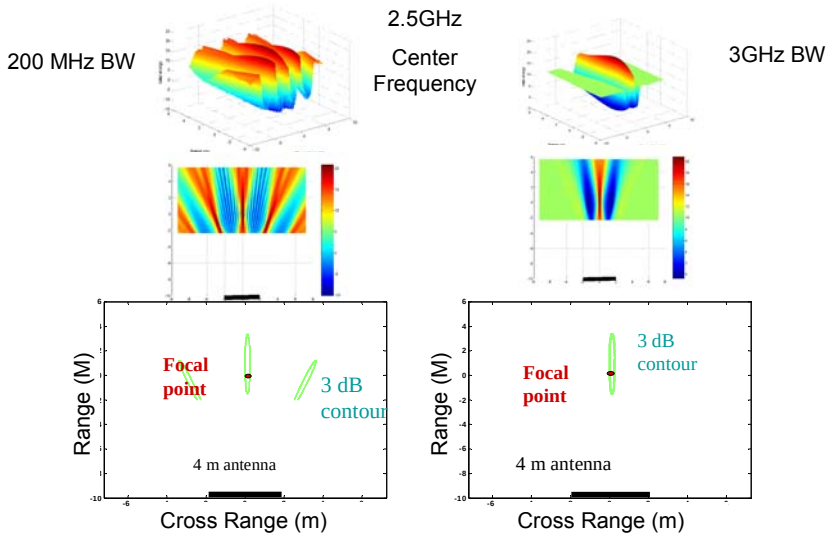

Figure 2 Example case comparison of the focusing ability of UWB signals as a function of bandwidth that will enable beam focus. (Left column-narrow band signals cannot focus. Right column-UWB signals enhance focus.)

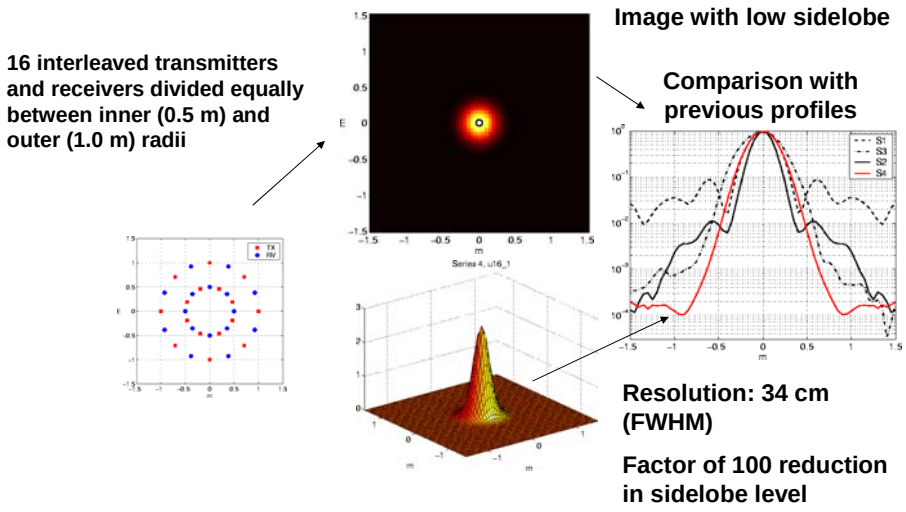

Figure 3 Example demonstrating the significance of array element distribution in suppressing the sidelobes that contributes to image quality degradations.

INTRODUCTION/BACKGROUND

In this LDRD project, our research purpose is to investigate the science and technology necessary to enable real-time array imaging as a rapid way to detect hidden threats through obscurants such as smoke, fog, walls, doors, and clothing. The goal of this research is to augment the capabilities of protective forces in concealed threat detection. In the current context, threats include people as well as weapons. In most cases, security personnel must make very fast assessments of a threat based upon limited amount of data.

Existing approaches have severe limitations in capabilities. In general, there are extreme tradeoffs between range of detection (especially through obscurants at distance), specificity, data processing time, and portability. An example on one extreme, metal detectors are fast but not specific; worse, they cannot detect non-metallic weapons and cannot be used to monitor human threats at a distance through walls. An example on the other extreme, backscatter x-rays are very specific but it cannot provide the data in real time and is thus of no use in tactical situations. It is also very large and cannot be used for field operations. In either case these techniques are detecting and screening for *objects* and do not have the capability to monitor in real time threatening actions of people through obstacles such as doors and walls.

In this project, we studied the use of real time (field programmable gated arrays) integrated with high resolution (cm scale), ultra wide band (UWB) electromagnetic signals for imaging personnel through smoke and walls. We evaluated the real-time imaging issues of detecting smaller objects such as concealed weapons that are carried by the obscured personnel. We examined the cognitive interpretation process of real time UWB electromagnetic images.

While two front end sensors can be used (acoustics and electromagnetics), we have selected to develop a beam forming and steerable ultra wide band (UWB) array for this effort. Among other attributes, UWB has been shown to penetrate many materials (wood, some concretes, non-metallic building materials, some soils, etc.) with very high range resolution. Further, we leveraged the LLNL UWB technical knowledge base and experiences gained through actual field deployments of monostatic systems to sites such as the World Trade Centers in New York (2001) to assist in the search and rescue efforts. We also collaborated with an expert from UC Davis in the field of cognitive sciences. Our approach was to formulate images in real-time that will engage the user's vision system in a more active way to enhance image interpretation capabilities.

Problem Definition

The objective of this project is to perform the research, development, and prototype refinement necessary for an entirely new way to rapidly detect hidden personnel at rest and in motion and evaluate the potential to detect concealed weapons with a high degree of resolution. The project will lead to a demonstration of portable-array, real-time imaging at multiple frames-per-second, which can detect personnel through smoke and simple structures such as doors. Started at mid-year FY02 through the SSEP directorate, we have advanced the process of refining the overall project requirements, developed functional algorithms for systems characterization and improvement, implemented the groundwork through computational modeling of the array performance, and developed the scientific principles for determining detection threshold and accuracy.

Troops and security officers responsible for Homeland Defense and Homeland Security, cannot easily detect hidden threats (*e.g.* movement behind walls, weapons under clothes). There is a need for new technologies to search for concealed threats; these technologies must be both fast and accurate, or there could be deadly consequences. Researchers have been largely unsuccessful at remote detection of concealed threats (personnel or weapons) with interrogating radiation (radar, millimeter-wave, acoustics, IR) either because of limitations of the modality (diffraction, jitter, reflectivity, noise/clutter issues, etc.) or clumsiness in the techniques (slow, unspecific). Entire conferences are being devoted to this problem, yet it still has not been satisfactorily solved. Radars, for example, require either long integration times or enormous computer resources to generate images. (All efforts to develop ground-penetrating radar land mine

detection systems and through barrier imagers have faced similar challenges.) Furthermore, the images produced are static, like a single frame of a videotape, so that uncorrelated noise and clutter dominate the scene. A way to reduce this noise is to average many frames, say by a factor of N, causing a decrease in averaged noise and thus improve signal-to-noise. However, in exchange for image quality, the detection is slowed. These noise and clutter issues are the leading cause of false detections; they are the main reasons these systems are still in the R&D mode and have never been deployed.

Instead of static images, why not make them dynamic? If the images are updated at video rates, again like a videotape, the human vision system processes out noise and clutter. Furthermore, if the observation point (the camera) is moved while taking pictures, we can get a three-dimensional "feel" of the scene (we can tell if a subject is near or far, for example). The problem is that we have not had the ability to process the data fast enough to handle the video rates. This problem has been the "holy grail" of array imaging, by LLNL and others, for the last decade.

Until now, dynamic real-time array imaging has been impractical. LLNL has built many transducer arrays for ultrasound, radar or multispectral applications, but we have been unable to produce multiple frames-per-second imaging. The problem has been accurate array timing, and fast signal processing. In the last two years, however, we have gained experience with recent field-programmable gate arrays (FPGA's) that appear to be capable of addressing both of these issues—accurate array timing and fast array signal processing. Significant issues still remain however (array size, spacing, wavelength, etc.) to produce the required detection accuracy.

Since the signals are 3D in nature (azimuth, elevation, and range or time), novel processing methods are feasible. The acquired 3D information can be sliced in various ways to produce real-time images in different cut sets (e.g., az-el, az-range, oblique angles, tomographic slices) or with multiple modalities to highlight features important to the search for concealed threats. Significant experimental testing, coupled with simulations, will be required to discover how real-time processing improves detection.

Site security is a priority at all significant installations. Also, military personnel and law enforcement officers place themselves in great danger to locate threatening individuals in obscured environments such as behind walls, doorways or underground. This research will enable a novel concealed threat detection capability. If successful, this research and its spin-offs will greatly benefit the Homeland Security effort, the military mission, and law enforcement.

Directorate Alignment

The SSEP Directorate has programmatic interest in improved threat detection. A real-time electromagnetic or acoustic camera will be an enabling scientific achievement because it will be unique in the world, and it will have enormous applicability.

Engineering, NAI and the former Laser Programs Directorate (now PAT) have developed a vast technology base around small impulse radar systems (MIR, or Micropower Impulse Radar). Many prior projects have successfully employed these patented radar systems for such applications as personnel security (DOE, DOD), bridge-deck inspection (DOT/FHWA), land-mine detection (Army), and helicopter blade tracking (Navy). Some of these systems employ arrays of radars, but with great difficulty in controlling the timing and great strain on computing resources. In other words, these systems either operate in real-time but are limited to single point sensors or provide reconstructed images but requires significant offline post signal processing. A strategic combination of these technologies to provide real-time imaging will benefit many programs.

Approach

We collaborated with an image perception expert at U. C. Davis for the research in human vision system, and we developed a research protocol for understanding detection capabilities. The technical approach is to first simulate in software the types of images that will be produced by a real-time array. Algorithms that can be fast yet produce technically interesting results will be implemented and tested; examples are motion analysis, clutter compensation, and noise suppression. We implemented imaging controls and algorithms into a simple array that can be controlled and measured in the lab. This system will help validate the simulation results. We demonstrated that such issues as timing, resolution, noise levels, and cross-talk are manageable, and that a full 2D hardware design is feasible. A brute-force solution to the data processing effort was implemented. New real-time imaging algorithms was designed. Detectability issues with respect to perception of real-time imaging was studied in controlled experiments. Publications and patenting the research results are pending. We worked with a number of DOD field staff to evaluate sub system capabilities in real-life structures. We will also continue our discussions with potential customers and future sponsors for this research.

We built upon five emerging technology elements to complete the goals of this research project— LLNL's electromagnetic (EM) simulation software, miniature radar transceiver technology from the MIR group (developed over 8 years), antenna array technology from the HERMES project (developed over 5 years), SmartCamera real-time processing capability (developed over 3 years in Energy and Engineering), and multiplexed timing capability from an on-going Engineering project (PI: Romero). This last technology is the final puzzle piece that makes the overall real-time array imaging and detection concept possible, though we will have to modify the FPGA board for our specific needs. The disciplines involved are human vision perception, EE and RF design, computer modeling, data analysis and statistics, real-time software design and systems integration.

This project has the following six major tasks:

1. *Simulation*: Develop/test a real-time array imaging simulation tool from existing static codes for both testing and design purposes. We will include real-time imaging errors and expected noise sources (diffraction, speckle).
2. *Algorithms*: Research new image processing methodologies and potential algorithms that can be preformed in real-time. A brute-force solution to the data processing effort will be initially implemented.
3. *Array design studies*: Use the simulation tool to test the sensitivity of various array designs; we will demonstrate that such issues as timing, resolution, noise levels, and cross-talk are manageable, and that a full 2D hardware design is feasible. Perform experimental analysis of the theoretical detection limits of real-time imaging versus static display.
4. *Real time integration*: Integrate laboratory array with FPGA system for real time imaging.
5. *Cognitive studies*: Measure the capability of human visual perception in real-time versus static imaging under various conditions. This step can start with simulated results, but will move to experimental data as hardware becomes available.
6. *Implementation plan*: Develop a plan for implementation of a full array for human perception studies and potential sponsor demonstrations. A University partner will be included in this work.

RESULTS/TECHNICAL OUTCOME

Psychometric Characterization (Visual Detection of radar Targets at Multiple Frames-per-second)

Introduction: The UC Davis project complements an Exploratory Research Project of the Engineering Division of LLNL. The goal of the LLNL exploratory research project is to determine the feasibility of acquiring and displaying radar images at multiple frames-per-second. The UC Davis research has for objective to establish basic design and performance characteristics for such a system from the standpoint of the detection of targets by a human observer.

There were three goals for the UC Davis effort:

1. To study the performance of alternative array structures that are feasible within the engineering constraints of the project.

2.To determine the characteristics of processed signals based on the array simulation results.

3. To carry out studies and simulations of the visual detection of targets using these signal characteristics.

We provide in this report an outline of our work and a summary of the results.

I. Array simulation studies

We made extensive use of the LLNL simulation software written by David Chambers to determine the capabilities and limitations of the radar imager. We considered the response of a single small scatterer so as to obtain the characteristics of the array imager. We summarize in this section the scope and findings of our simulation studies. Details are presented in Appendix.

As noted, we have taken as given and fixed the specifications of a single micropower radar (MIR). We considered a planar array of such MIRs and used beamforming as the imaging method. Such an array, which achieves a higher signal gain and a better spatial and temporal resolution than a single MIR is the centerpiece of the design of a real time radar imager. Starting with the specifications of a single MIR the design of the radar imager array requires consideration of:

The geometric configuration of the planar array.

A thorough investigation of the overall characteristics of the beamformed array has been carried out and is reported in detail in an appendix. The major results relate to the spatio-temporal resolution and to the effect of array aperture and configuration for rectangular and circular arrays.

IA. Array configuration

The spatio-temporal resolution of the array is principally determined by the frequency range and bandwidth of the transmitted signal and by the array configuration [2]. Since the MIR transmitted signal is known, beam-formed array configurations were simulated to determine that resolution. This work focused on two configurations: rectangular arrays and circular arrays. We determined that the circular array configuration gives consistently better resolution in the central lobe and comparable sidelobes with substantially fewer MIRs. Varying the number of MIRs from 25 to 9. We find that the resolution of the main lobe essentially does not decrease for circular arrays even for only 9 elements. However the sidelobes are only down by 10 dB for 9 MIRs as compared to 20 dB or more for 16 MIRs. Consistent with the requirement of a portable array, we considered principally a total array aperture of 0.6 meter. Under such conditions, the main lobe has a 3 dB width of 6 degrees, which corresponds to a resolution of approximately 0.4 m for a target at a distance of 4 m. This angular resolution is controlled principally by the aperture of the array. To generalize this specific

result, we also determined by simulation the effect of increasing the aperture on the angular resolution. We find that for a 16 MIR circular array the resolution in degrees is well approximated as inversely proportional to the array aperture. Thus the angular resolution could be lowered significantly within the limits of a mobile MIR array.

Another feature of the radar imager is the ability to time-gate the beamformed signal quite precisely. This capability may be exploited to control the resolution in range and possibly to decrease the angular sidelobes. The magnitude of the time response for a 16-element circular array can be used to infer that the 3 dB resolution in range is approximately 0.1 m and is essentially independent of distance. This range resolution is substantially better than the spatial resolution and will be exploited in the display processing. As expected, we have also observed a slight improvement in the angular resolution and a small reduction of sidelobes when a 50 pS time-gate is used.

IB. Signal processing alternatives and constraints.

In the processing of the MIR array signals to improve SNR and to increase resolution, we should note that the beamforming approach that we used is a generic approach that is effective and well suited to the scanning of the field of view for target detection. Improved discrimination of localized targets may be achieved by other methods, such as with the MUSIC algorithm, also available in the simulation software written by David Chambers. This more complex method is not necessary to carry out an engineering design investigation but should be considered in a final design stage. The temporal or range resolution may also be improved, as compared to time-gating, by exploiting more precisely the time structure of the received signals. The expected improvement may be significant, but it not essential for our present study. More importantly, good and consistent synchronization of the MIRs in the array is critical to beamforming or time-gating. This requirement was not explicitly tested, but the design jitter specification of 13 pS should result in a small degradation of the beamwidth. Since the resolution is principally dependent on the aperture, it should be noted that maintaining the synchronization of distant MIRs for a large array is needed for good performance.

II. Display processing and visual target detection.

Two studies were carried out in this part of our work: A comparative and quantitative determination of the detection of small targets in noise for several display strategies and simulations of the detection of targets from the signals obtained for a 16 MIR circular array.

IIA. Detection of small targets in noise.

This study extended and quantified the work carried during Summer 2002. It made use of the PsychToolbox that provides a calibrated display both in brightness and in frame rate [1].

1. Video display of a fixed target in noise:
In this experiment, we determine the visibility of the target as a function of frame rate. At each frame rate, the standard deviation of the noise was varied so as to bring the fixed target at the threshold of perception. The results are shown in Figure 4. We observe a rapid increase in threshold up to 20 frames/sec and then a progressive saturation so that increasing the rate above 30 frames/sec does not appear worthwhile. The figure demonstrates that video rate display at or above 30 frames/sec improves detectability by a factor of 2, or 6 dB as compared to a static display of the same target in random noise.

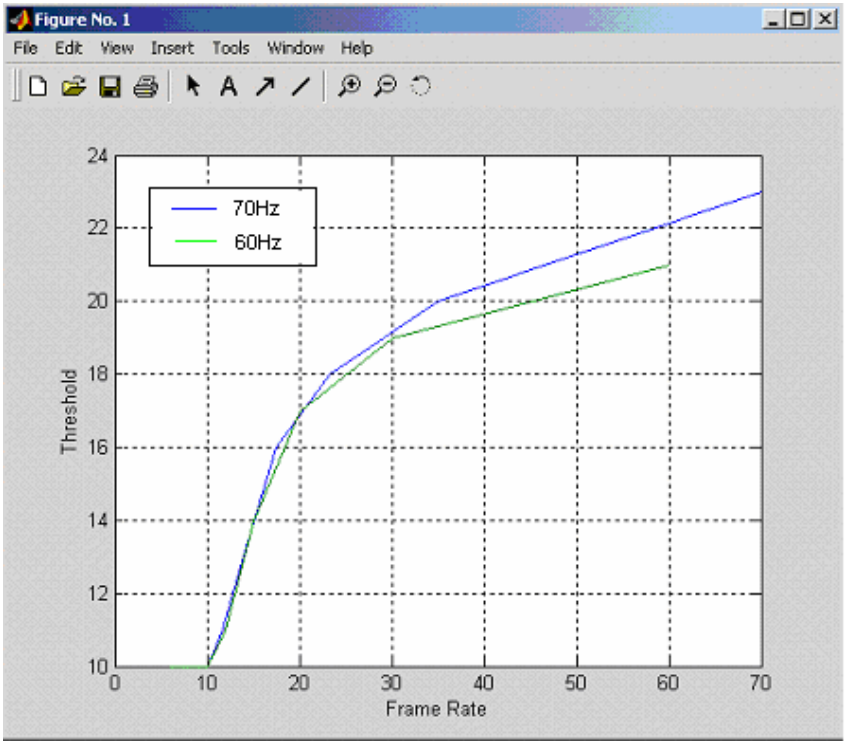

Figure 4. Threshold vs. frame rate in two different monitor settings

2. Detectability of several types of targets shape in noise.
We examined the effect of the shape of the target on its visibility in noise. The goal of this study is to set a basis for the choice of displayed shapes, which is possible when the acquired data is processed for display. The shapes were a dot, a cross, a line, a Gaussian spot and a 2D circle. There is a large difference in the visibility of targets of the same amplitude but of different shapes. We found

at the two extremes of detectability a dot that cannot be distinguished from noise and a line that is more readily detected at low amplitude. Here again we may observe an improvement in detectability by a factor of 2.

	SNR plot with threshold (dB)
Dot	4.8
Line	3.4
2D Circle	1.5
Cross	0.6
Gaussian Circle	0.2

Effect of target shape on detectability

3. Effect of target motion.

Building on these results, we conducted some experiments on the effect of the type of target motion on its detectability. We studied several target shapes that all provide similar results. Taking a small circle as the target, the types of motion were as follows:
a) Linear motion with overlapping circles
b) Linear motion with non-overlapping circles
c) Small motion in arbitrary directions.
We found that motion with non-overlapping circles was the most difficult to detect. The improved detectability for small motion and principally for the detection of linear overlapping motion is directly related to the visibility of a line that was discussed previously, since the motion a high frame rates transform overlapping motion into an equivalent elongated target.

4. Psychometric function for target motion.

We quantified the effect of the motion of the target by comparing the psychometric functions of a Gaussian spot undergoing motion for different types of motion. A forced choice experiment was conducted. In such an experiment, four adjacent panes are shown on the display. The target under motion is only present in one of the panes. The subject has to choose one of the panes as his or her best guess for the presence of the target. The probability of detecting correctly the target location will vary from 25 % for random choice, to 100 % for certainty. The curve of probability of detection versus target intensity is the psychometric function for that mode of target display. Here again the objective was to compare types of motions. The results are shown in Figure 4. The target with motion overlap was the most detectable and demonstrated that an improved detectability by a factor of 2 in amplitude as compared to large arbitrary motion non-overlapping of the target is possible. This is again relevant to high frame rates display where overlap of target positions in successive frames will occur.

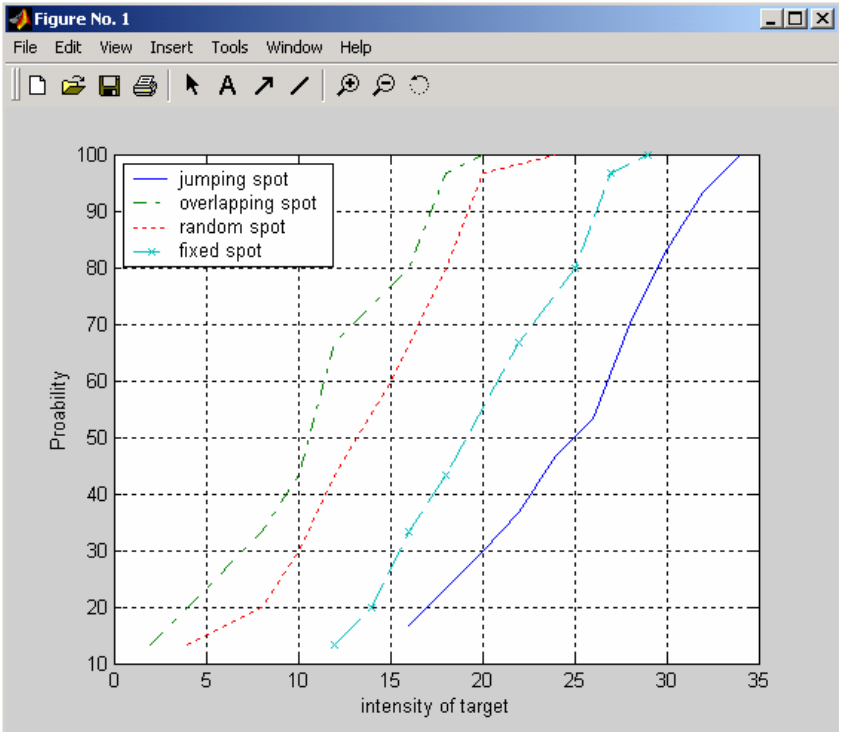

Figure 4. Psychometric function for moving targets

IIB. Conclusions on the detection of targets in noise.

1. The high frame rate of display for targets in additive noise improves substantially the detectability of the target. This is because the target is coherent from frame to frame and the noise is not. This result is achieved without any additional processing because human vision will essentially perform a temporal integration that reduces the visibility of random noise.

2. A display rate of 20 frames per second or higher is needed to achieve this improved detection for additive uncorrelated noise.

3. Elongated targets, or moving targets where the motion is incremental and overlapping on the display from frame to frame, will substantially be easier to detect than small fixed targets by a significant factor.

Based on these results we have investigated more realistic scenarios with simulated signals that approximate the expected output of a physical system.

III. Simulation of the detection of targets in noise and clutter for a circular array.

Based on the results we have reported, we chose the following system characteristics for an advanced simulation environment.

IIIA Array configuration and image acquisition parameters.

1. Array: 16 elements circular array with an aperture of 0.6 meter.

2. Spherical imaged region at a distance of 4 meters from the center of the array.

3. Angular sampling every 1.5 degrees or four times per main-lobe width. This means sampling every 0.1 m at the nominal imaged distance. The range is sampled every 0.1 m as well.

4. Imaged volume: We image a range of $\pm$ 30 degrees in both in azimuth and elevation and $\pm$0.3 m in range. We have therefore 40 X 40 X 6 samples in the imaged volume.

5. The entire data set is acquired in one thirtieth of a second.

6. Target size is 0.3m X 0.3m X 0.3 m and interfering scatterers are smaller in angle as well as in range than the resolution cell. Therefore the apparent size of the interfering scatterers is given by the resolution of the system. In particular, because of their smaller size the interfering scatterers will be detected only in one range bin while the target will be imaged over three or four range bins.

7. A target, several interfering scatterers as well as additive Gaussian noise are included in the simulation. We considered fixed or moving targets and fixed interfering scatterers.

IIIB Display alternatives.

The novel and interesting feature of the radar imager is the very rapid acquisition of three-dimensional data. In particular, the range may be acquired at a higher resolution than the returns in azimuth and elevation. This offers a number of opportunities to improve the performance of the imager. Since this three dimensional data set will be represented as two dimensional time varying images there are a number of alternatives in the ways the data set is processed and displayed. We examined some of these alternatives, guided by the results of our work on the detection of targets in additive noise. Since the final design and performance of the system will depend on lower level capabilities still to be resolved, the objective of this part of our work is to evaluate a flexible MATLAB

simulation environment that allows to readily test the alternate image display modalities. A simulation environment should also allow the use of successively more refined models for the target, the interfering scatterers or clutter and for the additive system noise. Within the scope of our study, a few processing/display alternatives have been examined for a fixed target and for a slowly moving target. These strategies take advantage of one or several of the visual perception results for still or moving targets in noise that we have described in the previous section: The reduction of the visibility of random noise at high frame rates, the effect of target shape on detectability, and the ease of detection of continuous, non random motion where the target overlaps from frame to frame. Because of the assumed characteristics for the range data, we have also exploited the coherence of the target across resolvable ranges, and the possibility to induce apparent target motion by interleaving range and angular pixels. As is the case in radar practice, in a radar imager several image display modalities should be available and exploited to increase performance for the distinct tasks of target detection and identification.

We comment briefly on the intent and performance of the following display modes that we have discussed previously or that we have explored in simulation:

1. Repeated display of a single range with no processing: This makes directly use of the reduced visibility of random noise at high frame rate that we have discussed previously. Although the random noise will be reduced, the unwanted scatterers will not be suppressed and would remain to be differentially resolved. This can be achieved if the target is in motion or if the scatterers differ from the target at different ranges.
2. Repeated display of successive range frames with no processing: This extends the previous mode by exploiting the coherence of the target across ranges. If the scatterers have range dependent characteristics, they will be reduced as compared to the coherent target.
3. Repeated display of the <u>average</u> of N_1 frames at a single range, N_1 =2-10. This method further exploits the random noise reduction property of the averaging operation. If the target is in motion, blurring will occur.
4. Repeated display of the average of N_2 range frames, N_2=2-6. By performing averaging over range frames, noise and scatterers, which are assumed to be smaller that the target, are reduced as compared to the target. Target motion will not lead to blurring since the same motion will occur for all the range pixels.
5. Interleaved display of four range frames as a single frame of twice the resolution. This is an interesting option for the assumed characteristics of the target and the scatterers. There are a number of alternatives on the interleaving of range and angular pixels. A simple method is to form a 2 X 2 pixels block from four successive range pixels at any angle. Thus four range frames will be combined into a single frame of twice the size. A target coherent across 4 range frames now appears twice larger than scatterers, which are only imaged at one of the ranges. This “snapshot across ranges” frame can be further processed in some of the ways outlined before if the target is in motion.

Other alternatives or modalities on the display of targets are possible and have to be tailored to the goal, such as a rapid scanning that minimizes misses, or a detailed view that should minimize false alarms.

IV. Discussion and conclusions

Although the major objective of the work at the CIPIC Interface Laboratory was on the design and evaluation of signal processing and display from the standpoint of the detection of targets by human observers, we have enlarged our work to include array simulation studies. This was necessary to obtain signal characteristics that were a reasonable first approximation to what a radar imager may provide. We believe that some significant results were obtained and insight was achieved from such array simulations. In the second phase of our work, we have carried out some systematic and quantitative studies of the detection of still and moving targets in noise and established the merit of high rate imaging both for still and moving targets. Finally, we developed and evaluated a simulation environment for the visual detection of still and moving targets for conditions that approximate a feasible radar imager configuration. Such a realistic and flexible software environment is necessary to refine and adjust signal processing and display characteristics to the evolving capabilities of the physical prototype.

V. References:

[1] V. R. Algazi and A.J. Angel “Visual Detection of radar Targets at Multiple Frames-per-second” Interim report on LLNL Intra-University Transfer (IUT) September 2002

[2] H.L. VanTrees: “Optimum Array Processing” Wiley 2002

PREDICTIVE MODELING

The work focused on a radio camera that scans a 200x200 pixel frame 30 times per second. The image is obtained by launching from a transmit array short ~ 2 ns UWB pulses to arrive at the desired pixel simultaneously. Similarly the receive array aligns the reflected pulses. For the purpose of discussion denote the scheme as the Focused Wide Band (FWB). FWB uses UWB pulses with a bandwidth larger than the carrier results to obtain clean focused spot as shown in Figure 5. The metric used is the total received energy of the signal, with the range^2 path loss normalized. Use of a carrier frequency larger than the bandwidth introduces grating spots. The spot size is a decreasing function of the aperture size, and the signal bandwidth. In the limit the spot size, i.e., the region within 3 dB from the maximum, is determined by the signal bandwidth and not the aperture size. An important feature of the FWB scheme is the uniformly low amplitude of side lobes for the ones not in the immediate vicinity of the main spot.

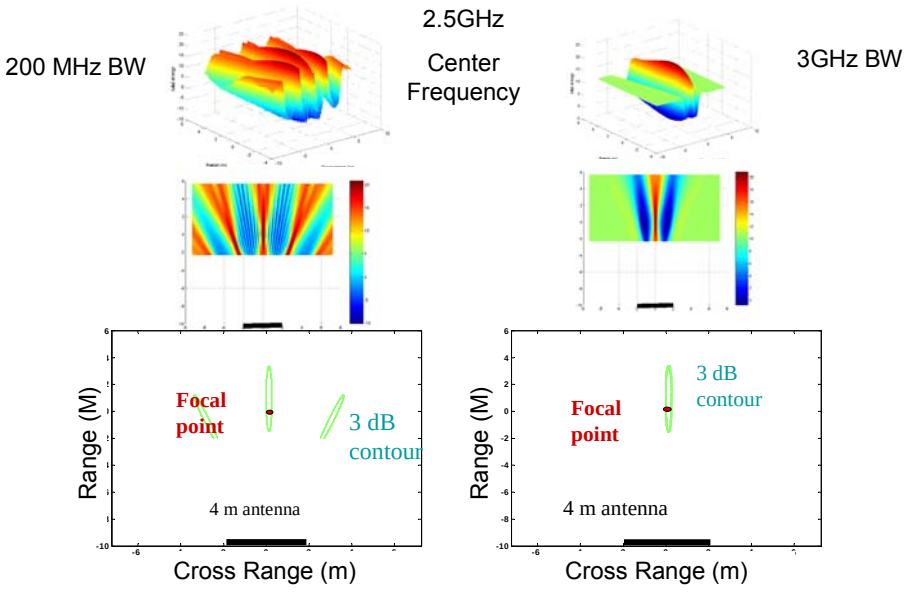

Figure 5 Example case comparison of the focusing ability of UWB signals as a function of bandwidth that will enable beam focus. (Left column-narrow band signals cannot focus. Right column-UWB signals enhances focus.)

The focusing capability of the FWB scheme was evaluated by a combination of experiments, simulation and analytic close form equations. A brief functional description of the test bed was given above. The greatest challenge in the test bed was control and compensation for the delay line error. The techniques learnt from the challnge will be very valuable in developing the radio camera. The FWB

experiments closely correlated with the simulation improving the credibility in both tools.

Two other schemes are possible to reduce the spot size. One denoted as the Hybrid Wide Band HWB, is signal based. In HWB the bandwidth of the signal confines the region where the spot might be formed. The size of the spot is determined, by the ratio of the carrier wavelength to the aperture size, as is the case in traditional narrow band systems. An illustration of such a scheme is in Figure 7.

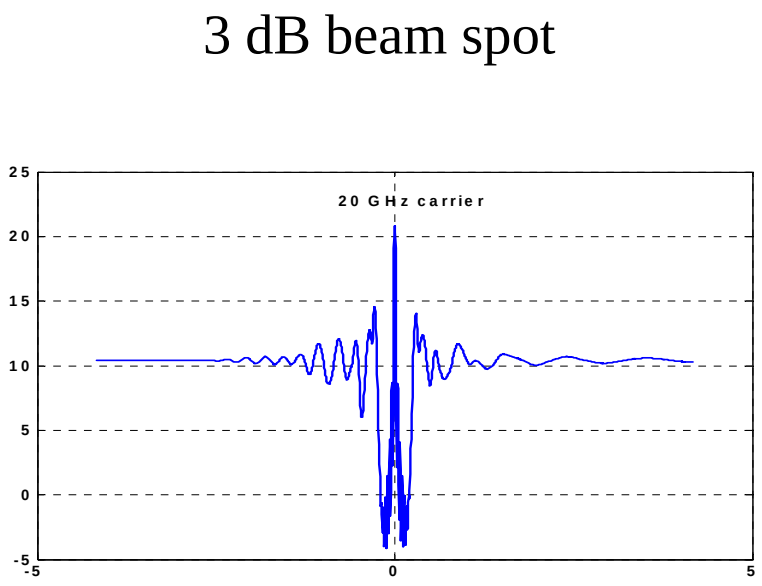

Figure 7 Example of grating spot (transverse view)

The second scheme denoted as the Widely dispersed Wide Band (WWB) is based on geometry of widely dispersed antenna elements. Consider the case of antenna divided into two clusters of contiguous elements, one is the transmit elements, and the other the receive elements. If the clusters have an elongated spot as shown in Figure 8, placing the clusters at the base corners of an equilateral triangle and have them point at the third corner would result in a smaller total spot size than if the clusters were collocated, as shown in Figure 9.

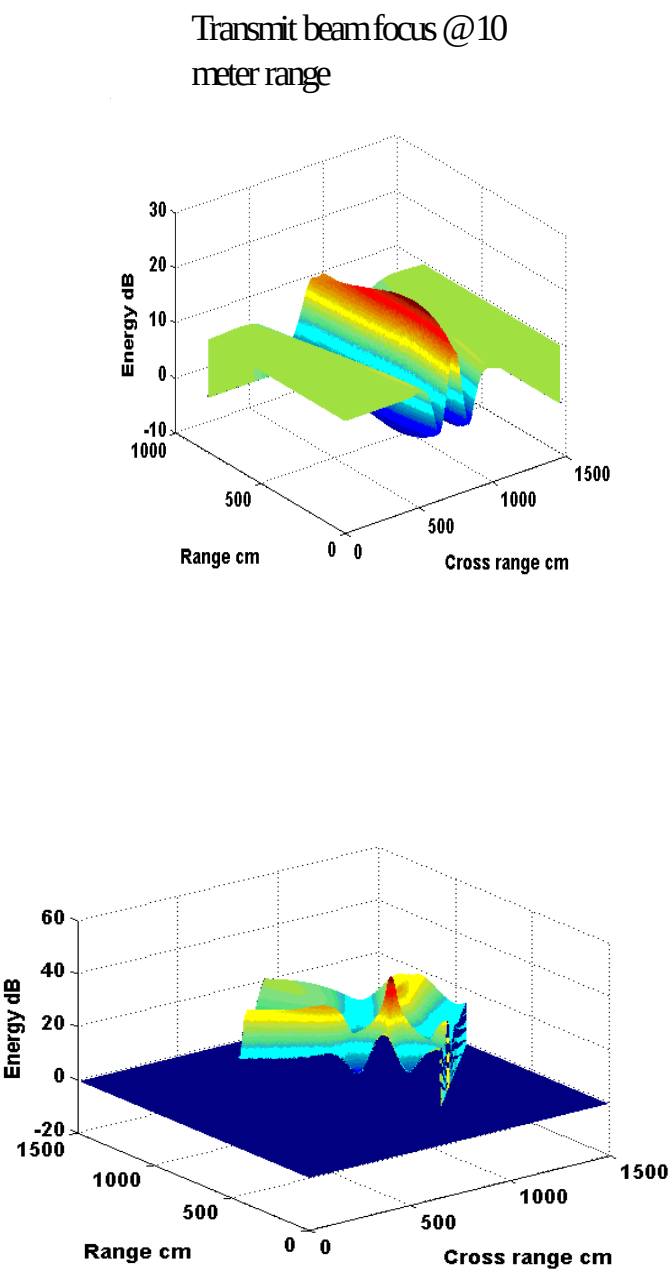

Figure 8 (top) and 9 (bottom) Cluster element placement demonstrates marked improvements on spot formation.

DESCRIPTION OF THE RADAR CAMERA PROTOTYPE AND ITS CURRENT CAPABILITIES:

Goals:

The radar camera system is designed to provide real-time images of a defined three-dimensional volume at a remote distance from the user. The use of UWB radio-frequency signals, centered about 2.2GHz, enables the user to locate and observe movement of targets obscured by walls, smoke, or other obstructions.

Hardware:

The system consists of an array of transmitter and receiver elements arranged in a vertical plane. At minimum, a single receiver and three transmitters are needed to identify positional information about imaged targets. The current system is capable of accommodating a total of 32 array elements. To date, eight elements (one receiver and seven transmitters) have been demonstrated. (More elements were not demonstrated because only eight were available at the time.) A future system is being designed to accommodate up to 32 transmitters and 24 receivers.

Transmitters:

When a transmitter receives a trigger signal, it emits an ultra wide band pulse centered about 2.2 GHz with a duration of roughly 2 ns. The shape of the pulse is described as a “Mexican hat”. These parameters are controlled by the shape and size of the antenna.

Receivers:

The receiver uses the same antenna as the transmitter. When a receiver is triggered, it samples the reflected signal energy for 70 ps. This window is narrow compared to the width of the peaks and troughs of the emitted 2ns pulse. The aim is to trigger the receiver at the time corresponding to the round trip time of an emitted pulse that is reflected from a known point in space.

Several custom-designed PCBs are used to control the timing of transmission and reception of RF pulses, the scaling and digitization of acquired data, and the display of data to the user. These are the controller board, the delay board, the gain board, and the display board.

Controller board:

The primary computation is the calculation of transmitter launch times and receiver sampling times to “scan” the defined volume or plane in space. Currently, these calculations are performed on a computer, and a “scan table” is loaded into memory on the controller board. In the future, these calculations will be performed by the FPGA on the board. The controller board directs all system timing, loads the appropriate timing delays onto the

delay board, loads amplitude scaling parameters onto the gain board, transfers received data to the display board, and communicates with the outside world.

Delay board:

Each delay board sets the timing of four transmit or receive channels. Multiple delay boards are used to control large arrays of elements. Each channel has a pair of delay chips that delay a trigger signal with 10 ps resolution. The range of the delay is from 0 to 20 ns. The scan table on the controller card specifies the desired delay value. Jitter of the timing signals has been measured at +/- 40 ps.

A significant challenge associated with using the digital delay system is that the delay increments are frequently larger or smaller than 10 ps. Step sizes ranging from –80 ps to +80 ps have been observed. These errors significantly impact the accuracy of the timing system, such that at a specified 20ns delay, the delivered delay can be off by 1 ns. Fortunately, the nonlinearities in the delay system are very repeatable, and therefore can be characterized using a lookup table.

Imaging Scheme:

Imaging is achieved by collecting return signals from a specified target plane. To image a volume, multiple planes are scanned and stacked. To scan a plane, all transmitters are timed such that their signals arrive at a single point in the target plane simultaneously. The receiver samples at the anticipated time a reflected signal should arrive. If a reflective surface is present at the point in the target plane, a high intensity signal return will be received. The system scans each point in the target plane in sequence.

Demonstrated capabilities:

- Scan a 2m x 2m plane at an offset distance between 1 and 2 meters.
- Scan three-dimensional volumes at 30 frames per second
- Scan 200 x 200 pixel planes
- Observed target reflections at distance of 6 meters

Human subjects involvment

This project evaluates a new imaging system to determine the feasibility of imaging the presence of human beings. The ultimate purpose of the project is to provide a new imaging method to be used as a search and rescue and concealed threat detection tool for the prevention of terrorism. The objective of the current research plan that involves human subjects is to test the instrumentation in being able to effectively create images of humans. The human subject research was approved by the Institutional Review Board.

Two human subjects were recruited for this study. The recruitment was done through posted flyers. All studies were done on LLNL property. An informational briefing were given to the volunteers. The human subjects were asked to stand or sit at least 3 feet in front of the imaging camera for a total of no more than 30 minutes at a time for no more than 60 minutes total. The camera consisted of ultrawideband radar transceivers that generate and receive electromagnetic signals that are orders of magnitude less than hand held commercial cell phones. There were no personally identifiable link between the identity of the individual and the data collected from the camera. The images captured corresponded to typical human behaviors such as walking, waving arms and legs, and holding light objects

The human subject research was exempted from the 45CFR46 policy for the protection of human subjects following the 45CFR46.101(b)2 policy for exemption of IRB review stating that:

45CFR46.101(b)2: Research involving the use of educational tests (cognitive, diagnostic, aptitude, achievement), **survey procedures**, interview procedures, or **observation of public behavior**

EXIT PLAN

We plan to apply our research results toward concealed threat detection for a number of interested sponsors.

Many of the new efforts are aimed at transitioning the results of this project to meet their programmatic needs. We've received seed to continue some of these efforts. We have been invited to submit white papers for seed efforts and full proposals for multi-year support. Based on extensive discussions with government agencies, we anticipate continuing development of mission-specific fieldable systems. There are several additional government customers who are aware of our program and are potential funding sources for follow-on to this work. We expect that patents and publications should attract industrial partnerships in the future.

ACKNOWLEDGEMENTS

Acknowledgement is made to the following individuals who have contributed to this project in provided mentorship, guidance, creativity, and dedication to the vision of this project over the years: Ellen Raber and Don Wentz of SEP; Harry Martz and Joe Galkowski, Annette MacIntyre of Engineering; John Woodworth as a Primary Reviewed of this work; Andrew Gertig of UC Berkely; Raymond Guan and Maggie Ko of UC Davis.

References

1. Netravali, A. N., and Haskell, B. G., Digital Pictures: Representation, compression, and standards. 2nd ed., New York : Plenum Press, 1995.
2. Goodman, J. W., Introduction to Fourier Optics, New York: McGraw-Hill, 1968.
3. Dougherty, E. R., and Laplante, P. A., Real-time Imaging, IEEE Press, 1995.
4. Hedrick, W. R., Hykes, D. L., and Starchman, D. E., Ultrasound Physics and Instrumentation. 3rd ed., Mosby, 1995.
5. Vickers, RS (ed.), Ultrahigh Resolution Radar, Proceedings SPIE, vol. 1875. Los Angeles, Ca. 1993.

PUBLICATIONS, CONFERENCES, AND RECORDS OF INVENTIONS

(Not exhuastive)

J. Chang, G Azevedo, Dave Chambers, Peter Haugen, Richard R Leach, Christine Paulson, Carlos E Romero, Alex Spiridon, Mark Vigars, James Zumstein. Ultrawideband Radar Methods and Techniques of Through Barrier Imaging. IEEE International Symposium on Antennas an Propagation and USNC/URSI National Radio Science Meeting, Monterey, CA. June 20-26, 2004. (Invited)

Alex Spiridon, G Azevedo, Dave Chambers, John Chang, Peter Haugen, Richard R Leach, Christine Paulson, Carlos E Romero, Mark Vigars, James Zumstein. Ultrawideband Spot Focusing. (Manuscript in preparation)

Dave Chambers, G Azevedo, John Chang, Peter Haugen, Richard R Leach, Christine Paulson, Carlos E Romero, Alex Spiridon, Mark Vigars, James Zumstein. Ultrawideband Radar Camera Simulator. (Manuscript in preparation)

Richard Leach, David Chambers, John Chang, Peter haugen, Carlos Romero, Leonid Tsap, Mark Vigars, Garth Pratt, Steven Azevedo, Greg Dallum, Patrick Welsh. Comparison of Ultra-Wideband (UWB) Pulse Transmission through Common Building Materials. (Manuscript submitted)

Several other peer review journal papers are currently under preparation.

Two records of invention and associated patents have been filed. Specifically:

Subject:	Disclosure and record of Invention
LLNL File No.:	IL-11263
Title of Invention:	Through Wall Motion Imaging, Tracking, and Discrimination of Multiple Human Heartbeats and Respiration Rates
	Richard Leach, Jr., Patrick Welsh, John Chang, 9/23/03 all rights reserved

Subject: Disclosure and record of Invention
LLNL File No.: IL-11285
Title of Invention: Fast Framing, Through Obstacle, Electronically Steerable, Dynamic Radar Imaging Array
Carlos Romero, James Zumstein, John Chang, Richard Leach

APPENDIX A: ARRAY SIMULATIONS

By Raymond Guan and Ralph Algazi

A1. Introduction

In order to carry out a study of alternative video display methods for the visual detection of targets, we made extensive use of the LLNL simulation software package to determine the physical characteristics of the radar imager. We present in this appendix the scope and findings of our simulation studies.

We take as given the specifications of an isolated micropower impulse radar (MIR) system, and we consider a planar array of such MIR systems with various numbers of elements. Such an array achieves a higher gain and a better resolution than a single MIR and its design is the centerpiece of the design of a real time radar imager.

Given the specifications of a single MIR unit the design of the radar imager requires consideration of:

1. The geometric configuration of the planar array.
2. The method of processing the received array signals.
3. The display of the output data as high-resolution video.

The geometric configurations of a planar MIR array is investigated first, with the aid of the LLNL simulator that creates the two dimensional image of a spherical target. The basic configurations that are considered are rectangular and circular.

An important new characteristic of the radar imager is the ability to do very fine time gating. This can be exploited to give the radar a fine range resolution. The coherence of images of a single target across different ranges can then be used to reduce background noise or clutter and to improve the detection of targets.

A2. Simulation Software:

A Matlab software package written at LLNL by David Chambers was made available to us. The parts of the software that we used extensively on this project are the Matlab scripts bfsphere2.m and bfspheretg.m. The two scripts are used

to simulate a two dimensional planar array radar and to generate a 2-D image of a finite size, uniform density spherical target across azimuth and bearing angles of ± 30 degrees. The difference between the two files is that the simulator bfspheretg.m incorporates the time gating ability of the MIR radar while bfsphere2.m does not. Time gating allows the determination of the range of the target.

For our study, the imaging method used is the beamforming method although the simulation program also allows the use of the MUSIC algorithm as an alternative [1].

A3. Simulation Results and Analysis:

In this work, we considered a number of arrays located in the x, y plane, and an isolated target or scatterer. We present comparative and informative results by using the following specific characteristics, unless noted otherwise:

Target Radius: 0.1 mm.
Coordinates (x,y,z) of center of target: (0, 0, 4) m.
Number of elements: 16
Circular Array with an aperture of 0.6 m.

A3.1.1. Introduction.

From the detailed results generated in the simulation, we can analyze the resolution[1] and the signal intensity as functions of the spherical target radius, of the target position, of the aperture of the array, of the number of array elements and of their geometry. An example of simulation results for a circular array geometry using the known spectrum of the transmitted MIR is shown in Figure A1. Note that in analyzing the maximum intensity, Imax(x), with a target size chosen arbitrarily, only the relative intensity change as a function of target position is meaningful.

A3.1.2. Effect of the radius of the spherical target.

In this simulation, the size of the spherical target was varied from 10^{-3} to 10^{2} mm. If the radius "a" of the target is 10 mm or smaller, we find that the resolution is approximately constant. As for the maximum intensity Imax of the received signal as function of the target diameter, a, we plot it in logarithmic scales and observe a linearly increasing function of slope of 6. This indicates a power law with an exponent of 6 for the relation of maximum intensity to target radius for small targets. These two results are shown in Figure A2.

Note that in order to avoid the situation where the distance between the center of the radar and the target, say Dz, is an exact multiple of one of the discrete frequencies present in the transmitted signal spectrum, Dz was chosen to be an irrational number, approximately equal to 4.19.

[1] Unless otherwise noted, "resolution" denotes the cross-range resolution

A3.1.3. Effect of the distance of the target.

As expected, the intensity of the detected signal decreases as an inverse power law when the distance or range is larger than the aperture of the array. The range resolution as a function of target position has two characteristics: 1) For distances smaller than the aperture, the range resolution worsens as the range decreases, and 2) when the range of the target is larger than the aperture, the range resolution is about constant as was expected for a fixed time-gate duration. These results are shown in Figure A3.

A3.1.4. Effect of the Aperture

The aperture is the primary parameter that affects the cross-range resolution. In a log-log plot of resolution versus aperture, we observe that the resolution is a linearly decreasing function, i.e. the larger the aperture the better the resolution. For the particular simulation of a circular array with 16 elements, an empirical equation can be obtained that relates the resolution r, in degrees, as function of aperture p, in meters

Different number of elements in the array and the array geometry affects the resolution slightly, but the aperture is the most important factor that determines the resolution. In general, the resolution will be about inversely proportional to the aperture.

A3.1.5. Effect of the Number of Array Elements

By increasing the number of elements in an array the first sidelobes move outward to higher azimuth, possibly out of the angular range of interest, or even beyond the MIR main lobe that the simulation has not taken into account. At the same time, the magnitude of the sidelobes decreases as the number of elements in the array increases. For example, Figure A5 shows a 9 elements rectangular array, where the first sidelobes occur at ± 21 degrees. They are about 3dB lower than the main lobe and the resolution is 5.05 degrees. By increasing the number of elements to 16, the first sidelobes are pushed beyond ± 30 degrees, the attenuation is about -4.5dB and the resolution is 5.52 degrees. Note that the resolution worsens slightly by increasing the number of elements. Similarly, for a 25 elements array, the attenuation in the sidelobes is now down to -12dB while the resolution is slightly poorer at 5.8 degrees.

A3.2. Comparison of Circular and Rectangular Arrays. We show on Figure A5 a comparison of rectangular arrays to circular arrays for 9, 16 and 25 elements. For circular arrays the resolution is about constant at 5.78 degrees. As a broad guideline based on such simulations we found that for circular arrays of 11 elements or more the sidelobes will be at least 15 dB below the main lobe.

A3.3. Effect on a Circular Array of Adding One Element in the Middle

With the addition of an extra element in the middle of a circular array, the resolution of the array is poorer, but the sidelobes are generally lower. However, the additional attenuation in the sidelobes is not a good trade-off for the loss of

resolution. Therefore, putting an element in the middle of an array is not recommended unless the total number of elements in the array is only 10 or fewer such that improving sidelobes attenuation is more important than the array resolution.

A3.4. Effect of the Planar Array Geometry.

In terms of resolution, the rectangular array is slightly better than the circular setup if the number of array elements is 16 or less. Note however that the rectangular-aperture array beam pattern is not isotropic and it differs considerably as the polar angle varies from 0 to 45 degrees as compared to the circular aperture array. The sidelobes suppression for the rectangular array is much worse than for the circular array. Simulations with nine or more elements in an array show that the circular array gives at least 8 dB in sidelobes attenuation. The better sidelobes attenuation of circular arrays is mainly contributed by the non-uniform spacing of the array elements when the elements are projected onto an axis.

Another practical consideration in choosing array geometry is that a circular array does not constrain the number of elements in the implementation; while we have to use 9, 16 or 25 number of elements in a rectangular array design. Therefore a circular configuration is recommended for the planar array geometry.

A3.5. Sidelobes Analysis

If the spacing between each element in the planar array is not small enough and the transmitted signal is narrow-band, grating lobes will occur [3]. For a wideband signal spectrum, the first sidelobes are actually a spectral weighted sum of the grating lobes.

For a uniform rectangular planar aperture and a single frequency plane wave model [2] with the main lobe at (0, 0) the first grating lobe will occur at an angle

$$\pm[\chi o\sigma^{-1}(\frac{300\,\delta}{\phi})-\frac{\pi}{2}]/\pi\cdot 180$$

degrees, where f is in GHz, and d is the smallest spacing between any array elements in mm.

For example, a 2 by 2 array with an aperture of 600 mm will have a spacing of d = 600 mm between adjacent elements. For a 2.2GHz signal, the grating lobes occur at +13 and -13 degrees.

If a more complex spectrum is used, as is the case in an MIR, grating lobes corresponding to different frequencies are located at different angles. This results in an attenuation as compared to the main lobe and we obtain broad attenuated sidelobes instead of grating lobes. However, the location of the first sidelobes can be approximated by the above formula with f equal to the center frequency of the radar transmitted signal spectrum.

For the circular planar array, the spacing of each element in any direction is non-uniform and this causes the first sidelobes to be lower than for an uniform rectangular array with the same number of elements. However as compared to a rectangular array, the resolution is slightly poorer for 16 or fewer elements.

A3.6. Locating the Target by Time Gating.

To locate the target position in three dimensions, the Matlab simulator bfspheretg.m is employed. Just as with the simulator bfspheres.m, it can generate a 2-D image across azimuth and bearing for spherical angles up to 35 degrees based on (round trip) time gate center tg_o. Time gating will provide the target distance or range as well so that using bfspheretg.m a 3-D volume of data is obtained. By finding the maximum value of the 3-D data, the corresponding tg_o provides the location of the target in range (z-axis) by the formula:

$$R_z = c \cdot \frac{tg_o}{2} \cdot \cos(A_b) \cdot \cos(A_a)$$

where c is the speed of light and A_β and A_α are the bearing and azimuth angles respectively.

It was observed from the simulation that both the resolution and sidelobes attenuation are improved by using time gating. For example, using time gating in a 16 elements circular aperture array of 0.6 meter aperture, the resolution improves from 5.8 degrees to 5.5 degrees and the side-lobes attenuation increases from -18dB to -20dB.

With time gating, range resolution is based on the characteristics of the time waveform for fixed azimuth and bearing angles. The simulator bfspherestg.m generates the square magnitude of the time signal and the 3dB width of that signal will determine the range resolution. Range resolution is thus independent of target range if it is larger than the array aperture. For a target located at 4 meters in front of a 16 elements circular array, the range resolution is about 0.1 meter.

A4. Discussion and Conclusions:

The characteristics of the MIR radar by use of the radar imager simulation have been analyzed and reported. Several conclusions can be drawn. For instances, from Figure A3 that shows the resolution as function of target position in the z-axis, it clearly suggests operation of the radar at a distance of at least the size of the array aperture in order to obtain optimum performance, at least for the beamforming imaging method. We also note that the simple inverse relationship between resolution and aperture can be used as the first approximation in the design of the MIR radar for a required resolution.

The simulation also has shown that a circular aperture is clearly the choice for the array configuration. It gives a consistent resolution for different number of array elements and results in acceptable sidelobes level with fewer elements. By taking advantage of time gating, a good range resolution can be obtained. This range resolution can be used to discriminate the target from clutter or noise and for the display, detection and identification of targets.

A5. Other Processing Strategies:

The performance characteristics of the wide-band radar can be improved by alternate processing strategies. For instance, the sampling and digitization of the received signal at the receiver-end can be exploited to optimize the array patterns by FIR filtering, when the FIR filter coefficients are obtained by optimization at different angles [4]. The potential advantage of such a method is that with the same number of elements in the array, processing by FIR filtering results in increased sidelobes attenuation while improving the resolution, which may be critical when only few elements are employed.

References:

[1] D.H. Chambers and J. G. Berryman (January 2003). "radar imaging of spheres in 3D using MUSIC." LLNL.Report

[2] H.L. Van Trees (2002). "Optimum Array Processing." Wiley.

[3] F. Anderson, W. Christensen, L. Fullerton and B. Kortegaard (August 1991). "Ultra-wideband beamforming in sparse arrays." IEE Proc.-H Vol. 138, No. 4.

[4] D.P. Scholnik and J.O. Coleman (May 2000). "Formulating Wideband Array-Pattern Optimizations." IEEE International Conference on Phased Array Systems and Technology, Dana Point, CA.

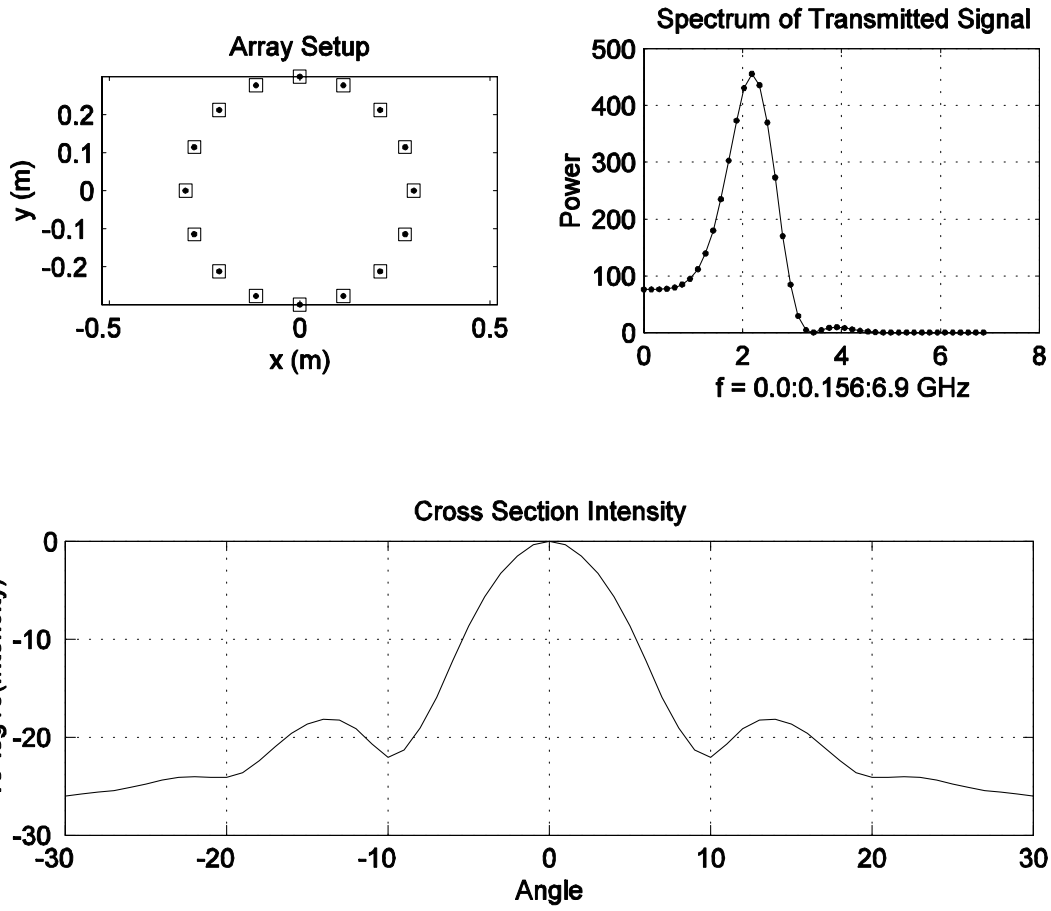

Aperture = 0.6 m

16 elements circular array

Target @ (0.0, 0.0, 4.0) m

Target (Sphere) Radius = 0.10 mm

Resolution is 5.7761 degrees or 40.31 cm

Image Angle = -30.0:1.00:30.0 degrees

R = 4.0 m from -10 to 10 degree is 1.4 m

from -30 to 30 degree is 4.0 m

rho0 = 10.0, rhos = 1.0, c0 = c, cs = 0.9*c

Imax = 2.858e-013 @ (0.00, 0.00) degrees

Average array sphere radius (rsphavg) = 4.0 m

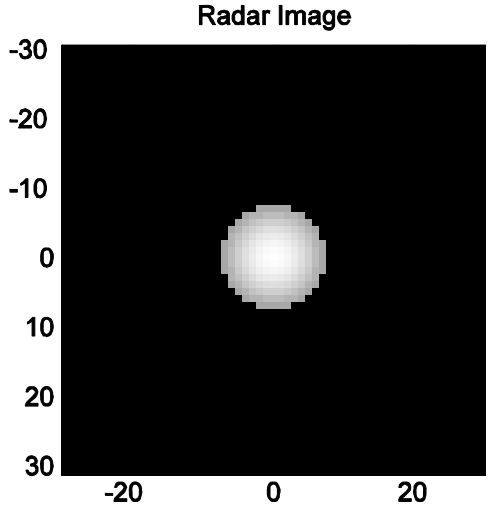

Figure A1. A 16 elements, circular aperture array setup and simulation result.

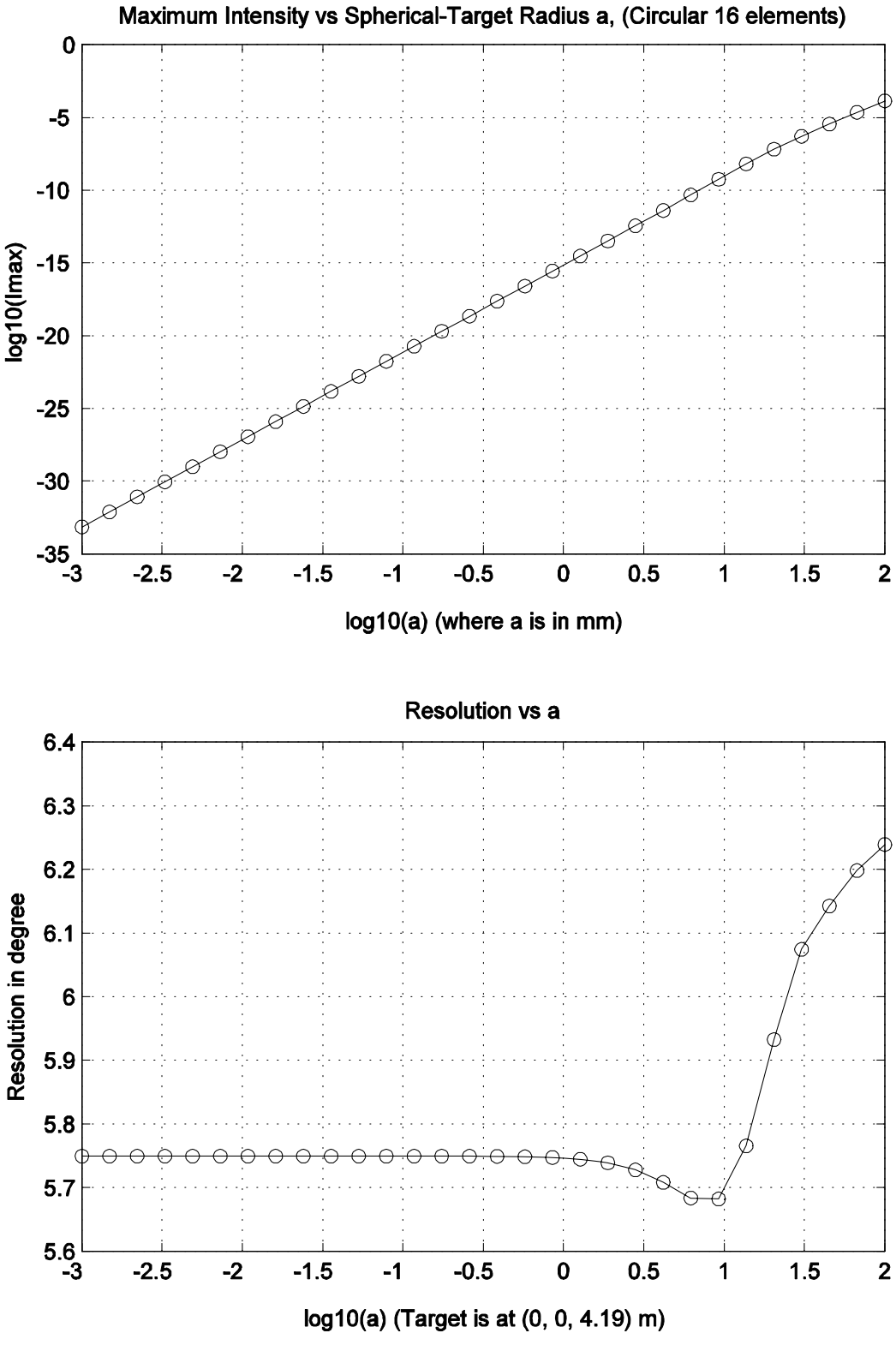

Figure A2. Maximum intensity and resolution as function of target radius.

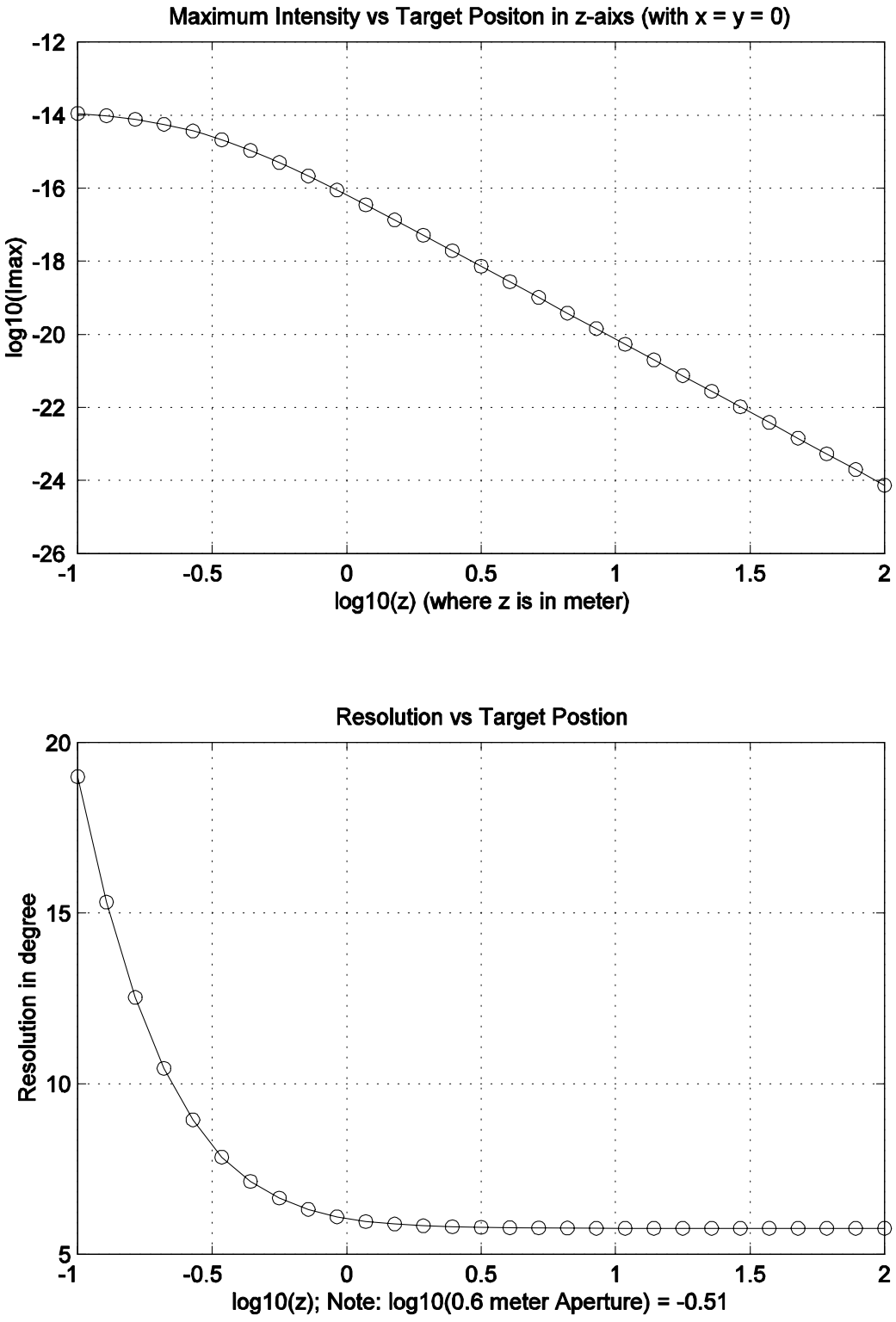

Figure A3. Maximum intensity and resolution as function of range z.

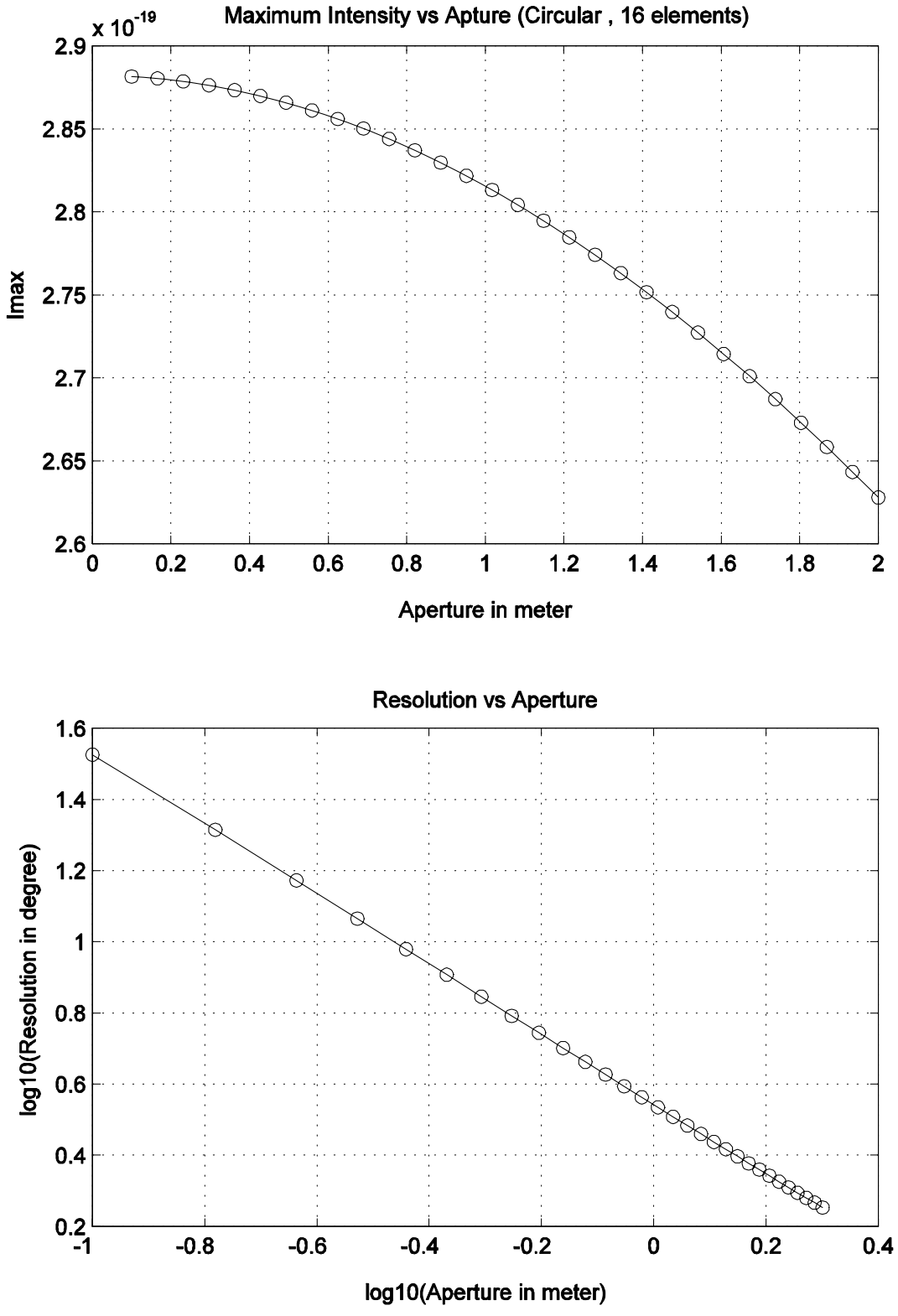

Figure A4. Maximum intensity and resolution as function of array aperture.

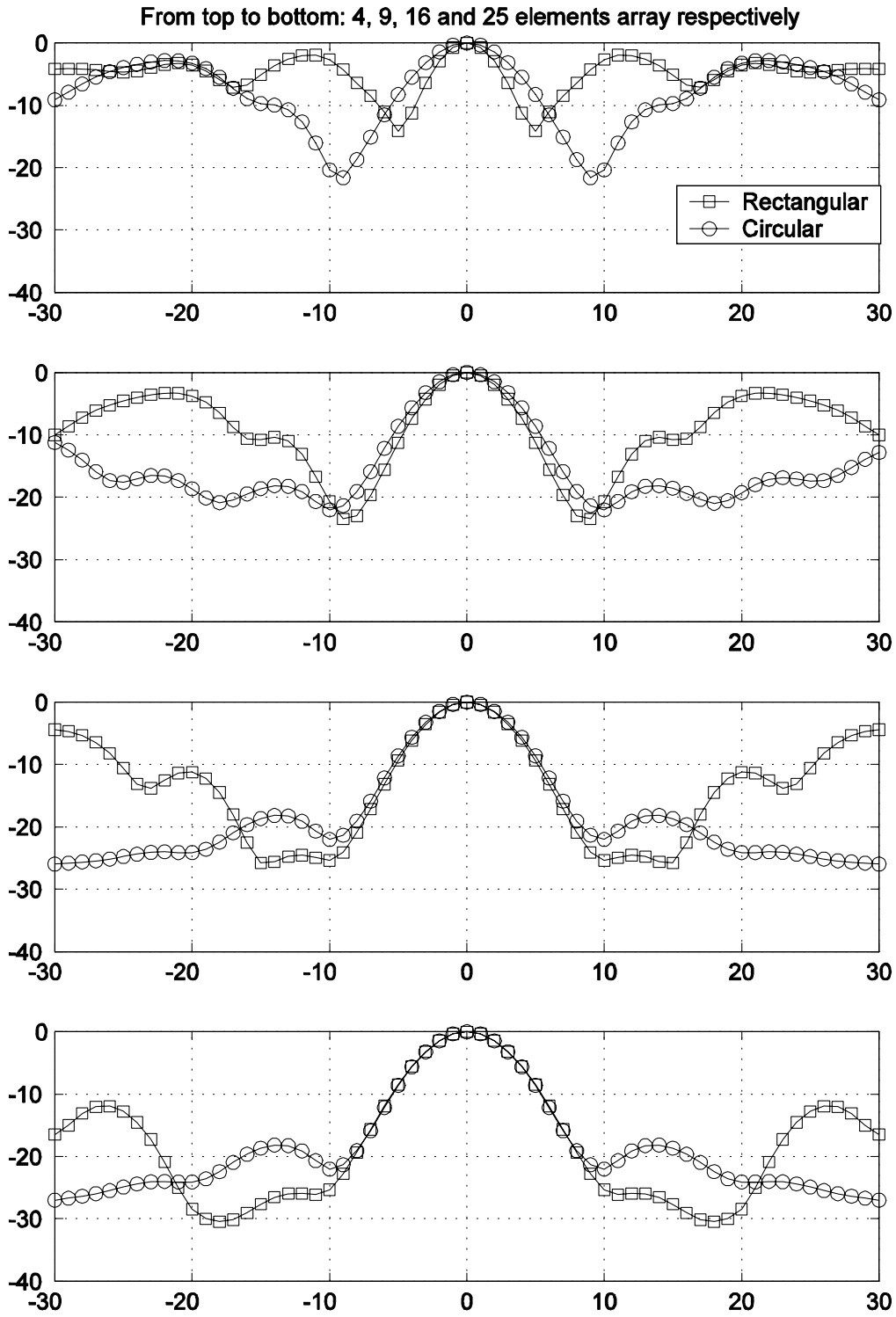

Figure A5. Comparison of 4, 9, 16 and 25 elements rectangular and circular arrays.

APPENDIX B: UWB ARRAY SPOT FOCUSING

Problem Definition

The problem addressed in this appendix is to determine the size of a beam focus spot for a linear array of N elements as a function of aperture size, the range to the focus point, and the signal bandwidth and carrier frequency. The size of the spot is determined in the plane specified by the linear array and the focal point. In contrast to the usual characterization of the beam by just its width the spot size is given both in range and cross range. The results are for focus points at boresight. Focusing off boresight is briefly discussed.

To characterize the beam spot shape, a metric for the signal strength is needed. The UWB beam signal consists of short pulses distributed over sporadic intervals of time. A meaningful metric of signal strength at a point is the total energy at a point, as the peak power might be deceptive for it might over a very short part of the pulse. In the evaluation the range^2 path loss term is normalized. The beam focus dwells on the link transmission, which by duality is the same on reception. Beam focusing is by control of the pulse transmission time. The array elements all transmit the same signal waveform SUW, from omni antennas. What the array does is adjust the transmission time from the array elements such that the signals from the different elements arrive at the intended focal point at the same time. Explicitly then if there are N antenna elements focused at a point P_f, then the signal received at a general point P_g, is given by

$$SG = \int \left(\sum_{i=1}^{N} suw_i \left(t - t_{gi} + \tau_i \right) \right)^2 dt \tag{0.1}$$

where suw_i is the pulse transmitted from antenna element i, t_{gi} is the delay from antenna element i to point P_g, and τ_i (tau) is the array time offset of element i.

When the general point fall at the focus point ideally τ_i (tau) is set equal to t_{gi} with P_g at P_f. Under this condition SF the focus spot strength has a value of

(0.2)

$$SF = \int \left(\sum_{i=1}^{N} suw_i \left(t_i \right) \right)^2 dt$$

$$= N^2 \varepsilon$$

where □ (epsilon) is the energy of a single pulse given by $\varepsilon = \int suw^2 dt$. At points far removed from the focus point, the likelihood of more than pulse overlapping is low resulting in a total energy of SG at them of N*□ (epsilon). This implies that N, the number of elements in the array, is the main beam to side lobe ratio at these points.

The results of beam focusing are directly applicable to communication links. For radar links combining the transmission and reception gain is only an approximation, as will be discussed later where more details on the target scattering angle towards the array are considered.

Pulse Dispersion

The time control of pulses is central to UWB array beam focusing, it impacts the size of the beam focus, and the level of side lobes. Consider determination of the 3 dB spot size, the location where the beam signal drops to half its peak value. An estimate is first obtained by adapting results from narrow band array. Nominally the 3 dB beam width is □D (lambda D) the ratio of the wavelength to the aperture width. At a off boresite angle at the edge of the 3 dB beam the signal from the center of the aperture is delayed with respect to that from the edge by DE where

$$DE = \frac{\lambda}{2D} * \frac{D}{2} = \frac{\lambda}{4} \qquad (0.3)$$

In an UWB pulse the signal is approximately one RF cycle, and is 2.5 ns long which is the inverse of its bandwidth of 400 MHz. The dispersion length for this Mexican hat pulse would then based on equation 1.3 have a value of 2.5/4=0.6 ns.

The above result for DE when evaluated for a signal of bandwidth BW I given by

$$DE = \frac{1}{4 * BW} * speed\_of\_light \qquad (0.4)$$

An alternate characterization of pulse train dispersion is next obtained by analysis of the wide band pulse itself, in the frequency and time domain. Ideally at the focal point the resulting pulse is N . UWF, while at a low side lobe the pulse train is dispersed in time and its energy low, for the aligned pulses, the energy is higher than when the pulses dispersed. For the purpose of analysis assume the dispersed pulses are spaced d meters apart. Let $SUW = \mathrm{F}(suw)$ then the Fourier of the train of pulses is given by

$$SUWt = SUW * \sum_{q=1}^{N-1} e^{-i(2q\pi fd/c)}$$

$$= SUW * \frac{1 - e^{-i(2N\pi fd/c)}}{1 - e^{-i(2\pi fd/c)}}$$

$$= SUW * \left(\left[\frac{Ne^{-iNd\pi f/c}}{e^{-id\pi f/c}} \right] * \left(\frac{\sin(2\pi Nd/(2c) f)}{N \sin(2\pi d/(2c) f)} \right) \right)$$

Noting Nd=De the total delay from first to last pulse then for $\pi df/c \approx 1$ (approx.~1) the value of ***SUWt is*** well approximated by the following expression

$$SUWt = N * e^{-i(N-1)df/c} * [SUW * \frac{\sin(\pi * f * De/c)}{\pi * f * De/c}] \qquad (0.5)$$

The above equation states the strength of ***SUWt,*** of dispersed pulses is mainly determined by the number of them N, the strength of an individual pulse ***SUW,*** and the total delay De over which they are dispersed. A corollary to this observation is the reduction of ***SUWt,*** from its peak value depends on De the equivalent distance separating the first from the last of the dispersed cluster of pulses. The distance De where the 3 dB drop from the peak occurs depends on the ***SUW,*** the pulse shape. For a nominal UWB pulse where the signal spectrum extends from 3/8 BW to a frequency 11/8 BW, the center of the pulse spectrum is at 11/16 BW. The sinc function $\frac{\sin(\pi * f * De/c)}{\pi * f * De/c}$ in Equation ddd, is a 0.44 *c/De Hz low pass filter. If the low pass filter bandwidth is to equal 11/16 BW then there will be a 3 dB drop as the low pass filter will only pass half of the pulse power. The following equality then applies

$$\begin{aligned} &11BW/16 = 0.44 * c/De \\ &\textbf{or} \\ &De = 0.44 * 16/11 * (c/BW) \\ &= 0.64\lambda \end{aligned} \qquad (0.6)$$

a value very close to that obtained in invoking the relation of wide band to narrow band system.

The above result used the frequency domain representations to evaluate the dispersed cluster of UWB pulses. A corresponding dual method is to use time domain analysis. A set of Mexican hat like UWB of 4 up to 16 in multiple of 4

were dispersed equally over a time interval T, noted energy drop from the peak value at T = 0 is independent of the number of pulse as predicted in the frequency domain analysis. Furthermore the value of T = 1.3 ns where a 3 dB drop occurs agrees with the value predicted by the 2 other methods

Relation to narrow band system

In several applications it is desirable to focus the array to a spot as opposed to just a narrow beam. The ideal focus is a single spot with very low side lobes every where else. This ideal becomes even more attractive if the constraint on array elements placement is relaxed with no penalty in introducing grating lobes. It is those features that the UWB is supposed to provide and will be discussed. In narrow band systems the signals from the individual elements are present almost continuously on and the signal temporal contribution to the array beam forming is only through the phase of a carrier at the different elements of the array. The phase control while allowing the array to form a beam does not prevent the waves launched from the different elements to interact with each other all over the illuminated space opening the possibility of forming unintended grating lobes. In stark contrast the very short limited time duration of UWB pulses launched from the different elements forms a small spot as the pulses collide with each other over a limited region. The array forms a focus at the spot, if it aligns the pulses from the different elements to arrive simultaneously at the spot. Their likely hood of re-aggregating at other points in space is small, and becomes even smaller the shorter are the pulses, i.e., the wider the bandwidth of the pulses.

To bring out this distinction between wideband and narrowband, consider this one dimensional toy illustrative example, using abstract narrow and wide band signals. The array consists of two point sources far separated one to the right and to the left, the array focuses its beam at the origin, i.e. at the point x = 0. In the first case, for the narrow band link they launch CW signals, a positive moving wave $P^{+}= e^{j(wt-kx)}$ from the left point source, and a negative going wave $P^{-} = e^{j(wt+kx)}$ from the right point. The resulting total wave given by $P^{+} + P^{-}= 2\cos(kx)e^{jwt}$ achieves the objective of focusing the beam at x=0, but inadvertently introduces periodic grating lobes, of amplitude 2, at x=n□(lambda) where □(lambda) is the carrier wavelength and n is an integer.

In the second case the array launches very wide band pulses by limiting the CW transmission, to a window wv, of width T approximately the inverse of the signal bandwidth i.e. where

$$WV = \begin{cases} 1 & for -0.5T < t < 0.5T \\ 0 & otherwise \end{cases} \qquad (0.7)$$

Using a T of one □ (lambda) the resulting beam amplitude as a function x, the 'range' where the maximum 2 possible for radiated is attained at x=0, the midway point between the radiating elements. The wide band signal greatly

reduced the spot size to T a length comparable to the inverse of the pulses bandwidth.

Another example is in order to bring out and further clarify the focusing capability of UWB arrays. It essentially builds on the above example for it consists of several pairs of diametrically opposing emitters lying on a circle. The array elements focus the beam to a spot at the center. The spot formed at the center, each diametrically opposed pair of array elements takes care of confining the spot along one aspect angle. Taking this result and combining with the above toy example discussion a basic attribute of UWB array beam focusing can be stated *The size of the focal spot is ultimately limited to light speed times the inverse of the signal bandwidth provided the bandwidth is larger than the carrier.*

Beam focusing spot size

The above results delimiting the region where the cluster of pulses drop by 3 dB from its peak is the basis of analytic models for spot discussed next. The analytic models are checked by explicit numeric simulation, and by controlled experiments, as discussed in section. The size of the spot is evaluated first at bore sight and, in Appendix A, off bore sight. The array width is 2 D meters, the focus point at point A, is v meters away. We compute first The 3 dB spot limited in azimuth by point B, W meters away from point A, where W is half the spot width. The pulse cluster transmitted from the right half of the aperture is limited in time by pulses from point P1 and P2. For pulses from these two points to arrive at point A at the same time, the pulse from point P2 should be launched ahead of point P1 by □A (delta A)where

$$\Delta A = \sqrt{R^2 + D^2} - R \tag{0.8}$$

At point B the propagation time difference from point P2 and point P1 is

$$\Delta B = \sqrt{R^2 + \left(D - W\right)^2} - \sqrt{R^2 + W^2} \tag{0.9}$$

At destination B the pulses from point P2 compared to those from point P1 have a transmission lead of □A (delta A), and a longer propagation delay of □B (delta B) which results in the pulses having a net spread of □Ã□B (deltaAdeltaB). This spread meets the 3 dB criteria as follows

$$\Delta A - \Delta B = De \tag{0.10}$$

Given R, D, and De, the above three equations provide a solution to W specifying the spot width.

We consider next computing the spot length along range. This is obtained by computing the range to BL and BU the inner and outer limits of the spot as depicted, given by L1 and L2 respectively. The equations for L1 and L2 are

similar to those for W. Consider first computing L1; at point BL, the difference of path length from P1 and P2 is

$$\Delta BL = \sqrt{L1^2 + D^2} - L1 \tag{0.11}$$

Combining this with the expression for □A (delta A), given by Equation 1.8, the following Equation for De holds

$$De = \Delta BL - \Delta A \tag{0.12}$$

Equations 1.8, 1.11, & 1.12 then specify L1.
In a similar the Equations for L2 are

$$\Delta BU = \sqrt{L2^2 + D^2} - L2 \tag{0.13}$$

$$De = \Delta A - \Delta BU$$

The length of the spot is then given by L2-L1. Explicit Equation for spot length is then given by

$$spot\_length = \frac{W^2 - \left(\sqrt{R^2 + D^2} - R - De\right)^2}{2*(\sqrt{R^2 + D^2} - R - De)} - \frac{W^2 - \left(\sqrt{R^2 + D^2} - R + De\right)^2}{2*(\sqrt{R^2 + D^2} - R + De)} \tag{0.14}$$

The equations for spot have to be solved implicitly.